New excitations in ^{142}Ba and ^{144}Ce: Evolution of γ bands in the $N = 86$ isotones

H. Naïdja,[1,2] F. Nowacki,[1] B. Bounthong,[1] M. Czerwiński,[3] T. Rząca-Urban,[3] T. Rogiński,[3] W. Urban,[3] J. Wiśniewski,[3] K. Sieja,[1] A. G. Smith,[4] J. F. Smith,[4] G. S. Simpson,[5] I. Ahmad,[6] and J. P. Greene[6]

[1]*Université de Strasbourg, CNRS, IPHC UMR 7178, F-67000 Strasbourg, France*

[2]*Université Constantine 1, LPMS, Route Ain El Bey 25000, Constantine, Algeria*

[3]*Faculty of Physics, University of Warsaw, Ulica Pasteura 5, PL-02-093 Warsaw, Poland*

[4]*Department of Physics and Astronomy, The University of Manchester, M13 9PL Manchester, United Kingdom*

[5]*LPSC, Université Joseph Fourier Grenoble 1, CNRS/IN2P3, Institut National Polytechnique de Grenoble, F-38026 Grenoble Cedex, France*

[6]*Argonne National Laboratory, Argonne, Illinois 60439, USA*

(Received 24 March 2017; published 2 June 2017)

New excited states in ^{142}Ba and ^{144}Ce are investigated by means of prompt γ-ray spectroscopy of the radiation following spontaneous fission of ^{252}Cf. Measurements of angular correlations and the observed branchings allowed the assignment of spins and parities with confidence. The new measurements are reinforced by shell-model calculations where energy levels, electric transitions, and magnetic moments are consistent with experimental data. The presence of collectivity in the $N = 86$ isotones is confirmed by clear signatures of soft triaxial γ bands in both nuclei.

DOI: 10.1103/PhysRevC.95.064303

I. INTRODUCTION

Studies of neutron-rich nuclei in the vicinity of the ^{132}Sn doubly-magic core are currently an active subject of nuclear structure research. Recent advances in radioactive-ion-beam facilities and detection systems provided access to many exotic nuclei in this region [1–8]. At the same time, the progress in the development of the effective interactions combined with availability of large-scale shell-model calculations has opened up a new era of successful theoretical approaches [9–16] to explore and gain more information from this region of heavy mass nuclei.

One of the interesting aspects of this region is the evolution of nuclear deformation. It is tied to the enhanced collective motion, exhibiting signatures of both quadrupole and octupole correlations. The most salient examples are the octupole band in ^{140}Xe [17,18] confirmed by the new results in [5], the presence of vibrational γ soft bands in ^{138}Te, ^{140}Xe [4], and in ^{146}Ba [6], and finally the identification of octupole bands in barium isotopes [7,19–21] and in ^{144}Ce [22].

Detailed spectra of the excited states and their electromagnetic properties are good probes for determining the degree of the collectivity, and some evidence was already inferred in the region. In this work we focused on the $N = 86$ isotones ^{142}Ba and ^{144}Ce, where the knowledge of excited bands is extended, with the measurement of new γ transitions, depopulating high-spin, excited states. Spins and positive-parity assignments of these states are compared to shell-model calculations, and the investigation of the quadrupole properties exhibits the occurrence of triaxial γ bands. In order to shed more light on the onset of deformation and collectivity in these nuclei, the static quadrupole shape deformations β and γ are evaluated using a simpler geometric model and constrained Hartree-Fock calculations in the shell-model basis.

The article is organized as follows: after the description of the experimental techniques and the review of new γ spectra of ^{142}Ba and ^{144}Ce in Secs. II and III, we outline briefly the shell-model overview in Sec. IV, where we present calculations of the energy levels and $E2$ and $M1$ transitions. The presence of collective γ bands in these nuclei is established and approved using the constrained Hartree-Fock shell-model method (CHFSM). The conclusions are gathered in Sec. V.

II. EXPERIMENT AND DATA ANALYSIS

To search for new excitations in ^{142}Ba and ^{144}Ce we used multiple-γ coincidence data collected with the Gammasphere array of germanium (Ge) detectors, in a measurement of prompt γ radiation following spontaneous fission of ^{252}Cf. We refer the reader to Refs. [23,24] for more experimental details. The present work provides improved data as compared to the analysis of earlier ^{248}Cm-fission data [19,21]. The progress was due to both higher statistics in the ^{252}Cf-fission measurement, as compared to the ^{248}Cm-fission measurement and higher, relative population of ^{142}Ba and ^{144}Ce in spontaneous fission of ^{252}Cf as compared to spontaneous fission of ^{248}Cm. This is illustrated schematically in Fig. 1, which shows on a logarithmic scale the number of triple-γ coincidences in the $6^+ \rightarrow 4^+ \rightarrow 2^+ \rightarrow 0^+$ cascades from the $N = 86$ isotones of interest. The high rate for ^{144}Ce following fission of ^{252}Cf is predominantly due to the population in β decay of ^{144}La. It is higher in the present 1 μs experimental coincidence-time window as compared to the 0.4 μs window of the ^{248}Cm fission data.

The data collected in the experiment have been sorted within various time windows into three-dimensional (3D) histograms of high dispersion, which allowed further progress as compared to the ^{248}Cm-fission data analysis [19,21].

A. Angular-correlation analysis for the Gammasphere data

Crucial for discussing the structure of nuclei are reliable spin and parity assignments to nuclear levels. We have

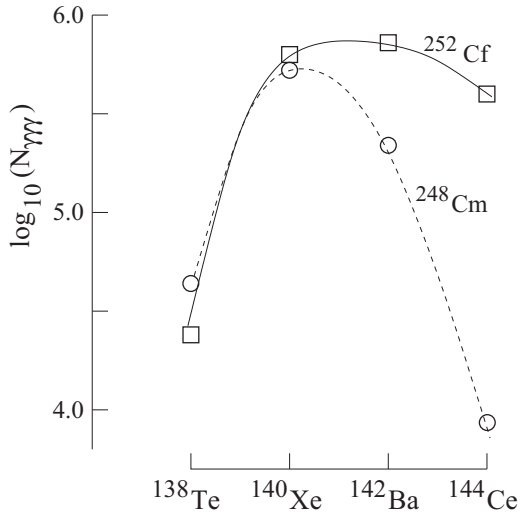

FIG. 1. Rates of triple-γ coincidences in $N = 86$ isotones observed in spontaneous fission of ^{248}Cm, reported in Ref. [4] and in spontaneous fission of ^{252}Cf, measured in this work.

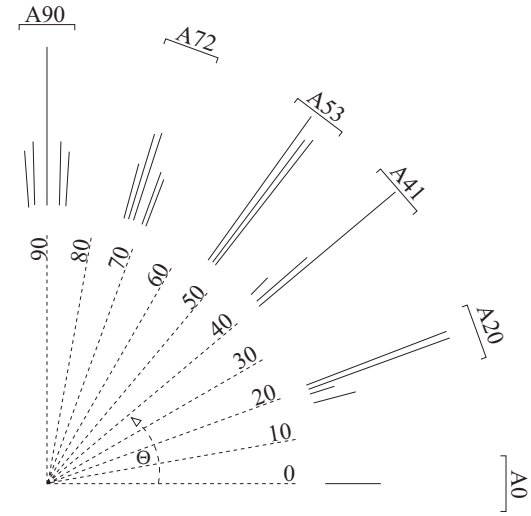

FIG. 2. Angles between detectors in Gammasphere. See text for further explanation.

developed a technique to determine angular correlations for $\gamma\gamma$ cascades following the spontaneous fission of ^{252}Cf, as observed with the Gammasphere array in the present measurement. This is analogous to the technique described in Ref. [25], where further information can be found.

Angular correlation function can be expressed as a series of Legendre polynomials,

$$W(\theta) = \sum_k A_k P_k(\cos\theta), \tag{1}$$

where θ is an angle between the directions of two γ rays in a cascade and P_k are the Legendre polynomials of rank k. The A_k values, which can be calculated using formulas of Ref. [26], depend on spins of levels and multipolarities and mixing ratios δ of transitions in a cascade. The A_k values calculated for various hypotheses, of spins and multipolarities in the cascade, are compared to their experimental values obtained from fitting formula 1 to the experimental intensities of $\gamma\gamma$ coincidences in the cascade at various θ.

It is convenient to normalize the formula 1 introducing new coefficients $a_k = A_k/A_0$. Because the experimental correlations are attenuated due to the finite size of the Ge detectors and the target, one has to introduce attenuation coefficients, Q_k, [27] multiplying the A_k coefficients (or normalized attenuation coefficients, $q_k = Q_k/Q_0$, multiplying the a_k coefficients). If the sizes and positions of the Ge detector crystals, relative to the target are known, the Q_k coefficients can be calculated rather accurately [25,27]. The updated formula (1) reads

$$W(\theta) = 1 + a_2 q_2 P_2(\cos\theta) + a_4 q_4 P_4(\cos\theta). \tag{2}$$

Using the angular coordinates describing positions of each of the 110 individual Ge detectors in the Gammasphere array, taken from the documentation [28], we calculated an angle between detectors for each Ge-Ge pair. In the present experiment 101 Ge detectors were placed in the array (9 positions were not used), providing 5050 different Ge-Ge pairs. Because of the high symmetry of the Gammasphere ball, there are "only" about 130 different angles in a range from 0 to 180 degrees. Various angular correlations were analyzed for Gammasphere in the past, using 20 angles in Ref. [24] or 17 angles in Ref. [29]. In this work we simplified the analysis using the symmetry of formula 2, where angles α and $180 - \alpha$ are equivalent, which allows to "transfer" the angles from the 90–180 range to the 0–90 range. Furthermore, some of these relative angles are rather similar, differing less than the angular "extent" of a single Ge detector. Therefore we grouped them, reducing the number of angles to be analyzed. The price to pay is that the size of the "effective detector" representing a given group is larger than the individual Ge detector, causing some increase of the attenuation coefficients, q_k. On the other hand the statistics in a γ spectrum corresponding to a group is significantly higher than for a single Ge-Ge pair.

We selected six distinctive groups of angles, containing about 70% of all Ge-Ge pairs. These groups, marked A0 to A90, are represented schematically in Fig. 2 by "bunches" of solid lines. The inclination of a line represents the angle, θ, between detectors, while the length of a line is proportional to the number of Ge-Ge pairs corresponding to this angle. For example, the line at angle 0° (group A0) corresponds to 50 Ge-Ge individual pairs of detectors, positioned at 180° ("vis-à-vis") in the Gammasphere ball.

As can be seen in Fig. 2, the number of Ge-Ge pairs varies from group to group. Furthermore, various Ge detectors were seeing γ radiation from the fission target differently because of extra devices around the target [23,24]. To compensate for these differences and other instrumental anisotropies, the normalization coefficients, $N(\theta)$, were determined for each of the group of detectors by fitting the formula (2) to isotropic angular correlations for 9 pairs of γ rays emitted in time coincidence from complementary fission fragments (for example, one γ ray corresponding to the 212.6-keV line of ^{100}Zr and the other to the 295.6-keV line in the complementary ^{148}Ce). Furthermore, we fitted 27 known, angular correlations

TABLE I. Normalization coefficients for various angles used in angular-correlation analysis of γ rays following spontaneous fission of ^{252}Cf, as obtained in this work. See text for further information.

Angle θ	Normalization $N(\theta)$
0.0°	0.078(1)
20.3°	0.741(3)
40.6°	0.646(3)
53.7°	1.200(4)
72.3°	0.945(3)
90.0°	1.000(3)

between pure quadrupole and/or dipole transitions in cascades, observed in nuclei strongly populated in fission of ^{252}Cf. This allowed a precise determination of the normalization coefficients and the attenuation coefficients, q_k. Table I lists the final values of $N(\theta)$ coefficients, obtained by averaging individual values from the 9 isotropic and 27 known angular correlations, shown in Fig. 3. The "Isotropic" points shown in Fig. 3 correspond to the average values obtained from the 9 individual, isotropic correlations. For most of these points, their uncertainties are smaller than sizes of the representing symbols. The q_k values obtained from fitting are $q_2 = 0.980(4)$ and $q_4 = 0.850(6)$. More information on this kind of analysis can be found in Ref. [30].

In Fig. 4 we show examples of known, stretched quadrupole-quadrupole (Q-Q), dipole-quadrupole (D-Q), as well as isotropic angular correlations, determined using the obtained $N(\theta)$ q_k parameters. The cases shown in Fig. 4 were not used for the $N(\theta)$ and q_k determination and illustrate high quality of the analysis procedure. Theoretical A_k values are $A_2 = 0.102$, $A_4 = 0.009$ for the QQ cascade and $A_2 = -0.071$, $A_4 = 0.00$ for the DQ cascade, while the corresponding, experimental vales are 0.092(6), 0.014(9) for the QQ case and −0.073(13), −0.007(19) for the D-Q case. For the isotropic distribution the experimental coefficients are $A_2/A_0 = -0.003(4)$ and $A_4/A_0 = -0.013(6)$.

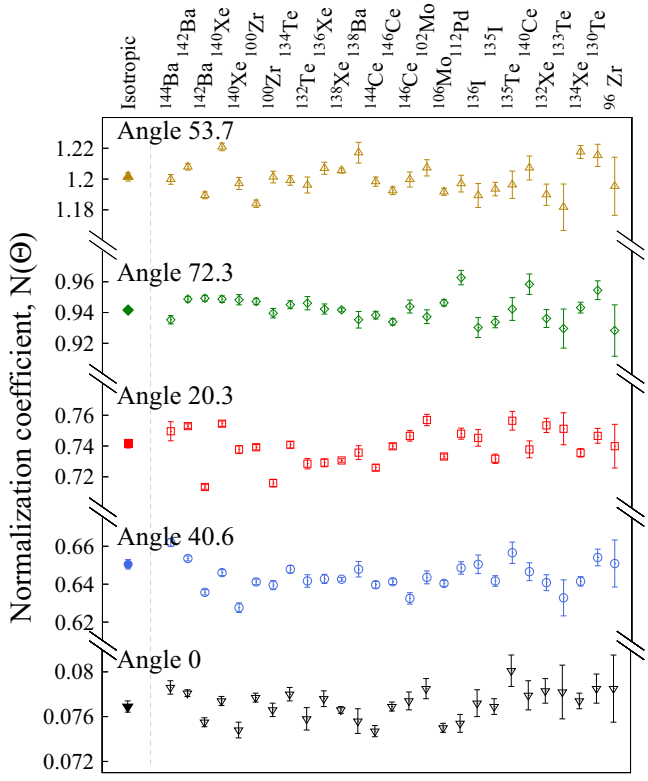

FIG. 3. Normalization coefficients for angular-correlation analysis obtained in the present work. See text for further information.

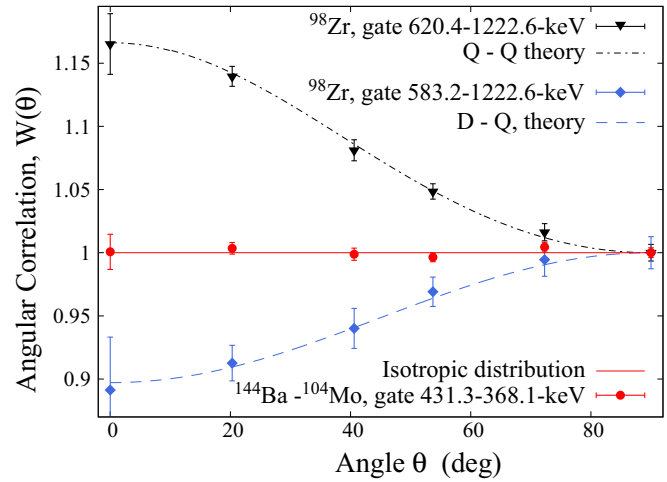

FIG. 4. Examples of angular correlations for QQ, DQ, and isotropic cases. See text for further information.

B. Level scheme of ^{142}Ba

A scheme of excited states in ^{142}Ba, populated following spontaneous fission of ^{252}Cf, is shown in Fig. 5. We confirm levels and transitions reported in the literature [31] and propose new levels at 1552.6 and 1601.5 keV at the bottom of the positive-parity, yrare band. In this band we also add a new level at 3963.1 keV. New, non-yrast levels are also introduced at 2132.7, 2276.4, 2410.7 3130.3, 3673.4, and 4294.8 keV. We add 19 new γ transitions, decaying from and to the new and the known levels. Properties of transitions in ^{142}Ba observed in the present work are given in Table II. The non-yrast levels, for example the 1326.1-keV level, are populated in the β decay of ^{142}Cs, produced in fission of ^{252}Cf. The intensities shown in Table II were derived from coincidence spectra, which provide accurate branching ratios but may not reproduce all the singles γ intensities properly.

Figure 6 shows a γ spectrum doubly gated on the 323.0- and 609.9-keV lines, corresponding to transitions in the positive-parity, yrare band of ^{142}Ba. This spectrum and other doubly-gated spectra revealed new lines of 145.5, 177.0, 195.7, 260.2, 309.21, 766.8, 1193.1, and 1241.8 keV. The new lines correspond to transitions linking the new 1552.6- and 1601.5-keV levels in this band to the known 359.55-, 834.70, 1292.36, 1424.0-, and 1747.2-keV levels.

Spin and parity assignments to levels in ^{142}Ba were determined in this work based on angular correlations, obtained with the technique described above, and the observed decay

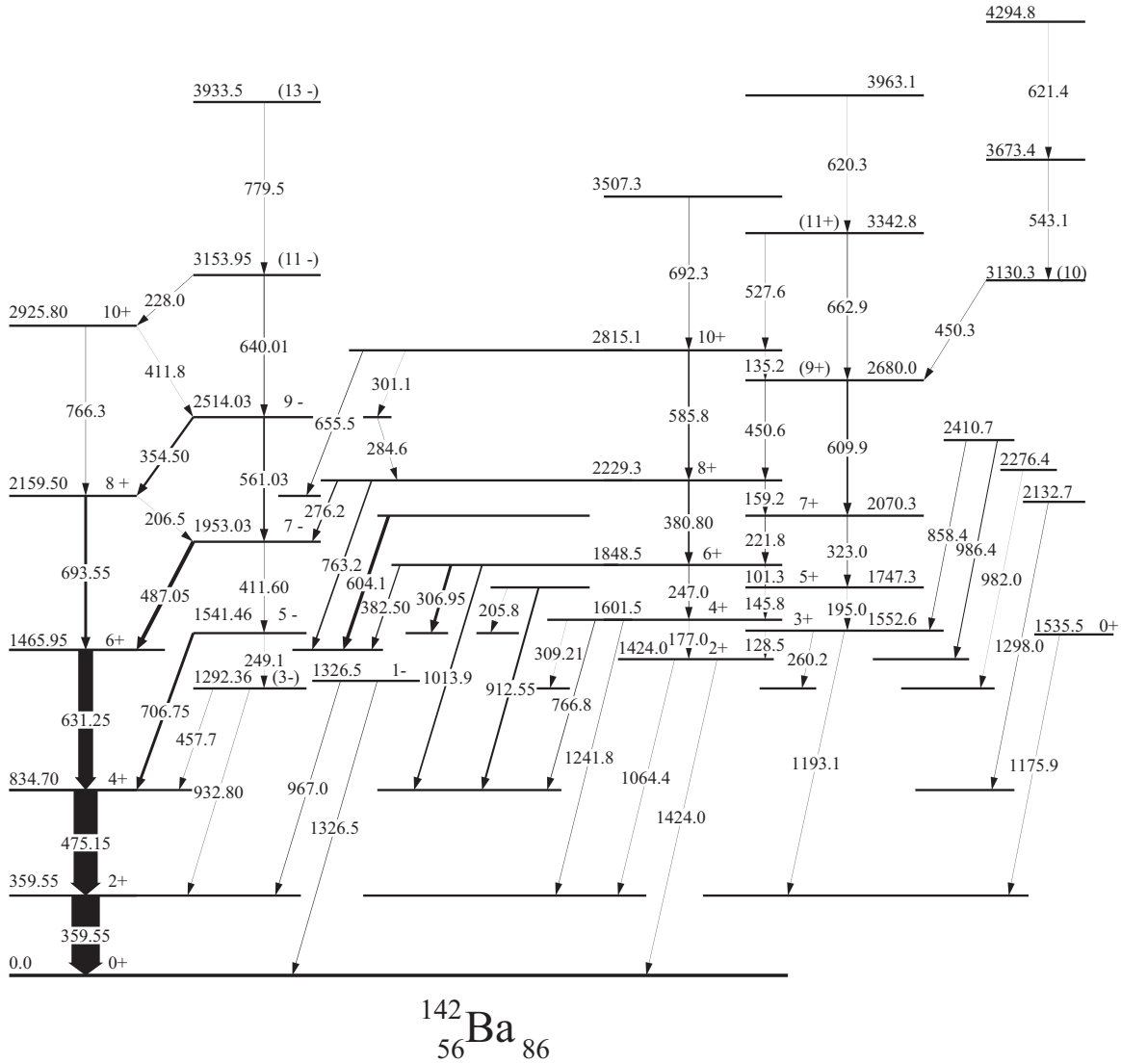

$^{142}_{56}\mathrm{Ba}_{86}$

FIG. 5. Level scheme of ^{142}Ba, populated following fission of ^{252}Cf, as observed in the present work.

branchings. We also took into account the well-documented observation of a predominant population of yrast levels in fission fragments [32]. At the bottom of Table III we show the angular correlation for the known 1175.9–359.55-keV, $0^+ \rightarrow 2^+ \rightarrow 0^+$ cascade from the second 0^+ state at 1535.5 keV in ^{142}Ba. Such cascades are characterized by a huge anisotropy, for which the theoretical coefficients are $A_2 = 0.357$, $A_4 = 1.143$. The agreement of the experimental and theoretical coefficients illustrates the high accuracy of our angular correlation analysis.

We adopted spin and parity 2^+, 4^+, 6^+, and 8^+ for the 359.55-, 834.70-, 1465.95-, and 2159.50-keV levels from the compilation [31]. Our angular correlations for transitions in the yrast cascades fully support these assignments, as seen in Table III. The correlation between the 766.3- and 631.25-keV transition confirm spin and parity $I = 10^+$, assigned to the 2925.8-keV level [31].

Our angular correlations are consistent with spin and parity 5^-, 7^-, and 9^- assignments to the 1541.46-, 1953.03-, and 2514.03-keV levels, reported in [31], though the fit for the 354.50–693.55-keV cascade is not satisfying (too large a_4). For the 3153.95- and 3933.5-keV levels tentative (11^-) and (13^-) assignments are proposed, respectively, based on the observed branchings and population. The 932.80–359.55-keV cascade is contaminated by the 931.8–358.8-keV cascade of comparable intensity, originating from ^{109}Rh. An analogous problem is encountered for the 457.7-keV transition. This precludes a unique spin assignment to the 1292.36-keV level.

For the 1424.0-keV level we take the spin and parity of 2^+ from Ref.[31]. Angular correlations for the 912.55–475.15-keV and 912.55–359.55-keV cascades are only consistent with spin 5 for the 1747.3-keV level, as reported in [31]. The mixing ratio $\delta = -0.27(2)$ for the 912.55-keV transition indicates an $M1 + E2$ multipolarity for this transition, considering its prompt character, seen in the experiment. This establishes a positive parity for the 1747.3-keV level. Similarly, the correlation for the 1193.1–359.55-keV cascade indicates a spin and parity of 3^+ for the 1552.6-keV level. Angular correlations

TABLE II. Energies and intensities of γ decays from levels in ^{142}Ba populated following spontaneous fission of ^{252}Cf, as observed in coincidence data in the present work. The I_γ values are in arbitrary, relative units, normalized to 100 at the 359.55-keV line.

$E_{init.}^{exc}$ (keV)	E_γ (keV)	I_γ (rel.)	$E_{init.}^{ex3c}$ (keV)	E_γ (keV)	I_γ (rel.)
359.55(5)	359.55(5)	100(5)	2132.7(2)	1298.0(2)	0.9(2)
834.70(7)	475.15(5)	85(5)	2159.50(9)	206.5(1)	0.6(2)
1292.36(8)	457.7(1)	1.0(2)		693.55(5)	11(1)
	932.80(5)	1.2(2)	2229.3(2)	159.2(2)	2.0(5)
1326.5(1)	967.0(1)	2.0(4)		380.80(5)	5.5(5)
	1326.5(2)	2.5(5)		276.2(1)	4.5(5)
1424.0(1)	1064.4(1)	0.7(2)		763.2(1)	5.5(7)
	1424.0(1)	0.9(3)	2274.4(3)	982.0(2)	0.4(2)
1465.95(8)	631.25(5)	52(4)	2410.7(3)	858.5(2)	2.5(8)
1535.5(3)	1175.9(3)	0.7(2)		986.4(1)	3.5(9)
1541.46(9)	249.1(2)	0.3(1)	2514.03(10)	284.6(1)	0.8(3)
	706.75(5)	10(1)		354.50(5)	8.1(9)
1552.6(1)	128.5(5)	0.4(2)		561.03(5)	6.2(8)
	260.2(1)	0.9(3)	2680.0(2)	450.6(1)	2(1)
	1193.1(1)	1.1(2)		609.9(1)	5.6(8)
1601.5(1)	177.0(5)	0.4(2)	2815.1(2)	135.2(2)	0.4(2)
	309.21(5)	0.3(1)		301.0(1)	0.4(2)
	766.8(1)	2.4(4)		585.8(1)	5.5(8)
	1241.8(1)	1.5(3)		655.5(1)	2.8(6)
1747.3(1)	145.8(2)	0.5(2)	2925.80(12)	411.8(1)	0.5(2)
	195.0(4)	0.5(2)		766.3(1)	1.5(5)
	205.8(1)	0.6(2)	3130.3(4)	450.3(2)	1.5(5)
	912.55(5)	6.3(6)	3153.95(15)	228.05(5)	1.6(3)
1848.5(1)	101.3(1)	0.9(2)		640.01(6)	2.7(5)
	247.0(1)	1.9(3)	3342.8(2)	527.6(1)	0.9(3)
	306.95(5)	10.5(7)		662.9(1)	2.5(8)
	382.50(5)	4.5(5)	3507.3(3)	692.3(1)	2.0(5)
	1013.9(1)	6.0(5)	3673.4(5)	543.1(2)	1.0(5)
1953.03(9)	411.60(5)	1.5(5)	3933.5(2)	779.5(1)	0.8(3)
	487.05(5)	14(1)	3963.1(4)	620.3(3)	0.5(2)
2070.3(1)	221.8(2)	2.3(3)	4294.8(5)	621.4(2)	0.6(3)
	323.0(1)	2.1(3)			
	604.1(1)	12(1)			

for the 766.8–359.55-keV and 1241.8–475.15-keV cascades indicate uniquely spin 4 for the 1601.5-keV level. The large δ value of the 766.8-keV transition indicates positive parity for this level. The correlation of the 1013.9-keV transition with the 359.55- and 475.15-keV transitions indicates uniquely spin 6 for the 1848.5-keV level. Positive parity is due to the $E2$ multipolarity of the 247.0-keV transition, indicated by its prompt character. Other correlations shown in Table III and the observed branchings allowed the assignment of spins and parities to the band on top of the 1424.0-keV level, as shown in Fig. 5, making it a good candidate for a γ band.

C. Level scheme of ^{144}Ce

A partial level scheme of excited states in ^{144}Ce, populated following the spontaneous fission of ^{252}Cf, as observed in this work, is shown in Fig. 7. The properties of levels and decays

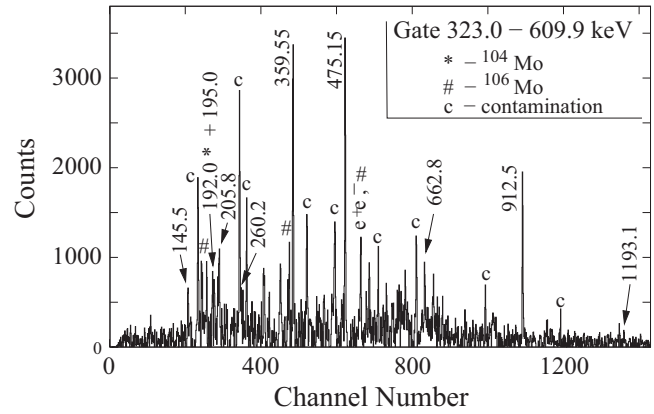

FIG. 6. γ spectrum doubly-gated on the 323.0- and 609.9-keV transitions of ^{142}Ba, obtained from a histogram of triple-γ coincidences following fission of ^{252}Cf. The quadratic energy calibration applied (constant-peak-width calibration) is strongly nonlinear with coefficients $A_0 = 0.11$ keV, $A_1 = 0.666\,667$ keV/channel, and $A_2 = 0.000\,155\,179$ keV/channel^2.

are listed in Table IV. In Fig. 7 we show only part of the scheme, relevant to the discussion of γ bands in the $N = 86$ isotones. High-energy levels, populated in β^- decay of ^{144}La will be discussed elsewhere.

As seen in Fig. 1, the population of ^{144}Ce is dominated by the β^- decay of the (3^-) ground state of ^{144}La. This is due to the high cumulative yield of this isotopes in fission of ^{252}Cf. However, direct population in fission is also present, allowing

TABLE III. Experimental angular-correlation coefficients, A_k/A_0, and the corresponding mixing ratios, δ, for γ transitions in ^{142}Ba, as obtained in the present work. "sum" indicates a correlation determined from a spectrum being a sum of γ spectra gated on the 359.55- and 475.15-keV lines.

Cascade E_γ - E_γ	A_2/A_0	A_4/A_0	Spins in cascade	$\delta(\gamma^a)$
323.0 - 912.55[a]	−0.172(20)	0.008(29)	7 → 5 → 4	−0.25(6)
				−2.4(4)
380.8 - 1013.9	0.095(18)	0.053(25)	8 → 6 → 4	
354.50[a] - 693.55	−0.061(9)	0.085(13)	9 → 8 → 6	0.02(2)
450.3[a] - 609.9	−0.129(34)	0.066(48)	10 → 9 → 7	−0.09(6)
475.15 - 359.55	0.102(4)	0.006(5)	4 → 2 → 0	
487.05[a] - sum	−0.050(9)	0.009(11)	7 → 6 - sum	0.04(2)
585.8 - 763.2	0.077(14)	−0.011(19)	10 → 8 → 6	
631.25 - sum	0.104(5)	0.027(9)	6 → 4 - sum	
693.55 - sum	0.100(8)	0.024(11)	8 → 6 - sum	
706.75[a] - sum	−0.068(7)	0.009(12)	5 → 4 - sum	0.01(1)
763.2 - sum	0.084(8)	0.000(12)	8 → 6 → 4	
766.3[a] - sum	0.038(8)	0.121(13)	4 → 4 → 2	−2.3(2)
912.55[a] - sum	−0.247(8)	0.001(12)	5 → 4 - sum	−0.27(2)
1013.9 - sum	0.103(9)	0.0014(14)	6 → 4 - sum	
1193.1[a] - 359.55	−0.402(38)	−0.084(51)	3 → 2 → 0	−1.2(5)
1241.8 - 359.55	0.105(42)	0.013(62)	4 → 2 → 0	
1175.9 - 395.55	0.358(41)	1.132(58)	0 → 2 → 0	

[a]Indicates γ transition for which the mixing has been determined.

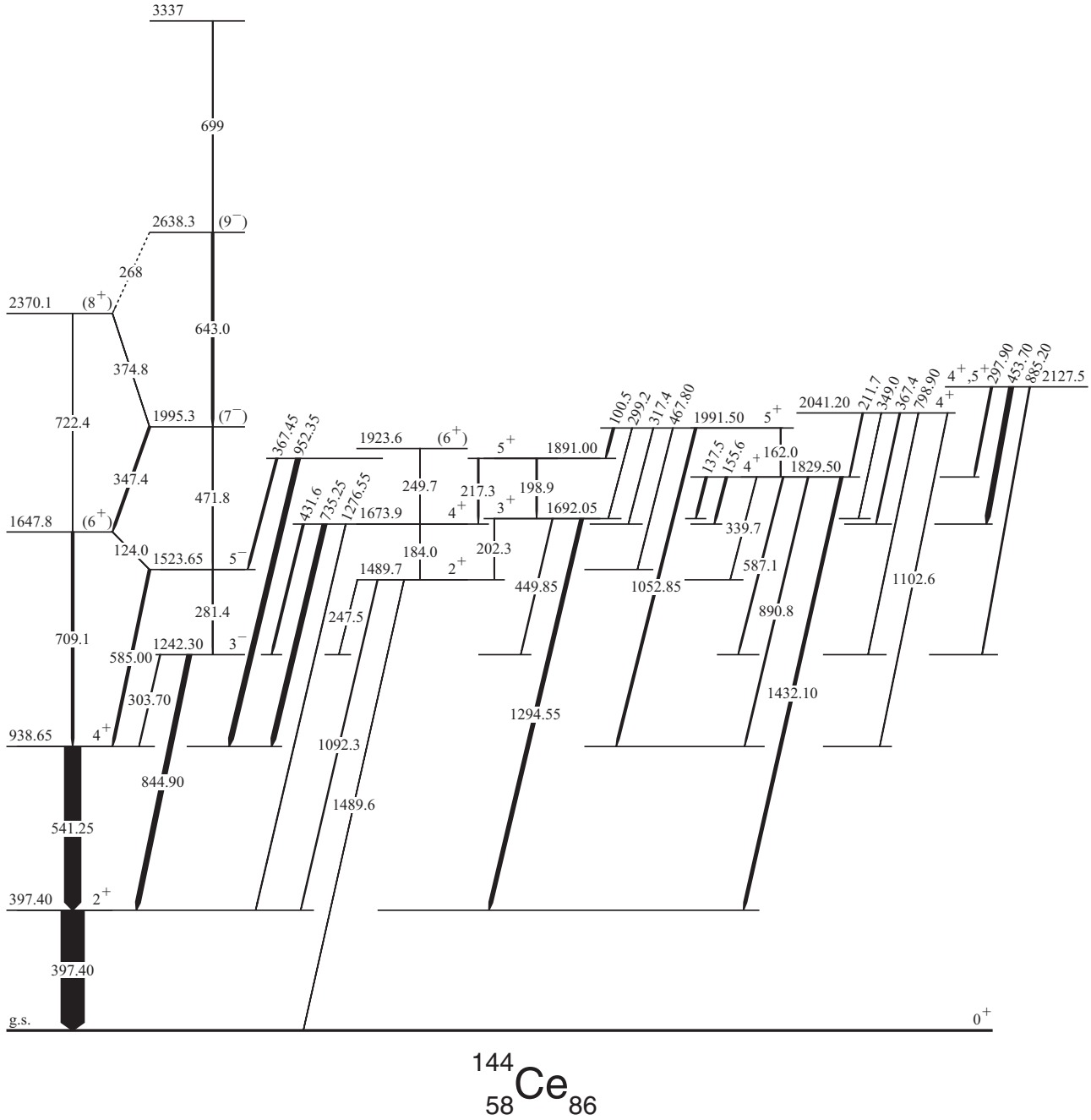

FIG. 7. Partial level scheme of ^{144}Ce, populated following fission of ^{252}Cf, as observed in the present work.

the observation of levels up to spin $I = 11$ in the octupole band. The non-yrast levels receive negligible prompt population from fission of ^{252}Cf. The intensities shown in Table IV were derived from coincidence spectra, which provide accurate branching ratios but may not reproduce all the singles γ intensities properly.

Levels and transitions of ^{144}Ce shown in Fig. 7 were reported in the literature [33]. We add a new level at 1923.6 keV. The important new results obtained in this work concern spin and parity assignments in ^{144}Ce which are based on angular correlations and the observed branchings. Details of this analysis are collected in Table V.

From the compilation in [33] we adopt a spin and parity of 2^+ for the 397.40-keV level. Our results confirm a spin and parity of 4^+ of the 938.65-keV level and uniquely define spin $I = 3$ for the 1242.30-keV level. A negative parity for this level is consistent with $\delta \approx 0$ of the 303.7- and 844.90-keV transitions. Similarly, a spin-parity 5^- assignment is made for the 1523.65-keV level. Tentative assignments to higher-energy levels in this band are proposed based on the observed branchings, assuming that spins are increasing with energy [32]. The new results indicate the presence of an octupole band in ^{144}Ce, resulting from the coupling of an octupole phonon to the ground-state cascade.

TABLE IV. Energies and intensities of γ decays from levels in ^{144}Ce populated following spontaneous fission of ^{252}Cf and β decay of ^{144}La produced in fission of ^{252}Cf, as observed in coincidence data in the present work. The I_γ values are in arbitrary, relative units normalized to 100 at the 397.40-keV line.

$E^{exc}_{init.}$ (keV)	E_γ (keV)	I_γ (rel.)	$E^{exc}_{init.}$ (keV)	E_γ (keV)	I_γ (rel.)
397.40(5)	397.40(5)	100(5)	1923.6(2)	249.7(1)	5(1)
938.65(7)	541.25(5)	90(5)	1991.50(9)	100.5(1)	0.7(2)
1242.30(7)	303.70(5)	3.5(8)		162.0(2)	0.2(1)
	844.90(5)	41(3)		299.2(2)	0.3(1)
1489.7(1)	247.5(2)	3(1)		317.4(2)	0.5(2)
	1092.3(1)	2.5(4)		467.80(7)	1.1(2)
	1489.6(2)	3(1)		1052.85(5)	5.0(5)
1523.65(9)	281.4(3)	1.7(3)	1995.3(3)	347.4(1)	0.6(2)
	585.00(5)	22(2)		471.8(1)	0.3(1)
1647.8(2)	124.0(2)	3(1)	2041.20(15)	211.7(1)	1.1(3)
	709.1(1)	9(1)		349.0(1)	5.4(8)
1673.9(1)	184.0(1)	2(1)		367.4(1)	8(1)
	431.6(1)	14(2)		798.90(7)	2.6(4)
	735.25(5)	18(2)		1102.6(1)	4.0(5)
	1276.55(8)	3.3(5)	2127.5(2)	297.90(7)	0.9(3)
1692.05(7)	202.3(3)	0.7(3)		453.70(5)	8.1(8)
	449.85(8)	0.9(3)		885.20(8)	1.5(5)
	1294.55(5)	9.7(9)	2370.1(4)	374.8(2)	0.6(2)
1829.50(8)	137.5(2)	0.3(1)		722.4(2)	0.3(1)
	155.6(1)	4.1(6)	2638.3(4)	268(1)	0.1(1)
	339.7(2)	0.4(2)		643.0(2)	3.0(5)
	587.1(1)	2.0(4)	3337(1)	699(1)	0.4(2)
	890.8(5)	4.8(8)			
	1432.10(7)	7.4(7)			
1891.00(15)	198.9(1)	7(1)			
	217.3(1)	2.5(5)			
	367.45(7)	7.4(8)			
	952.35(5)	10(1)			

A firm, 4^+ spin-parity assignment to the 1673.9-keV level results from angular correlations involving the 735.35-keV transition, in accordance with Ref. [33]. Due to the 184.0-keV link to the 1489.7-keV level with spin $I = 2$ [33], the parity of the latter level is positive. Unique 3^+ and 5^+ assignments to the 1692.05- and 1891.00-keV levels are based on angular correlations involving the 1294.55- and 952.35-keV transitions, respectively. These data indicate that the cascade on top of the 1489.7-keV level in ^{144}Ce is a good candidate for a γ band. We also see a number of 4^+ and 5^+ levels around 2 MeV of excitation energy, with firmly assigned spins and parities, which are strongly linked to the proposed γ band.

D. Angular correlations for ^{140}Xe

In this work we have also performed analysis of angular correlations for the key $\gamma\gamma$ cascades in ^{140}Xe complementing the analysis reported in Refs. [4,5]. The results shown in Table VI confirm the spin and parity assignments in ^{140}Xe reported in Ref. [4]. The value of $\delta = 0.21(11)$ favors an $M1 + E2$ character for the 820.7-keV transition, thus positive parity of the 2775.3-keV level in ^{140}Xe.

TABLE V. Experimental angular-correlation coefficients, A_k/A_0, and the corresponding mixing ratios, δ, for γ transitions in ^{144}Ce, as obtained in the present work. "sum" indicates correlations determined from a spectrum being a sum of γ spectra gated on the 397.40- and 541.25-keV lines.

Cascade E_γ - E_γ	A_2/A_0	A_4/A_0	Spins in cascade	$\delta(\gamma^a)$
303.70[a] - sum	−0.099(14)	0.013(20)	3 → 4 → 2	−0.04(2)
453.70[a] - 735.25	−0.027(9)	0.002(13)	4 → 4 → 4	0.47(2)
			5 → 4 → 4	0.14(1)
541.25 - 397.40	0.099(5)	0.003(7)	4 → 2 → 0	
585.00[a] - sum	−0.080(7)	0.006(10)	5 → 4 - sum	−0.01(1)
735.25[a] - sum	−0.042(5)	0.050(7)	4 → 4 - sum	0.68(2)
			5 → 4 - sum	No
844.90[a] - 397.40	−0.070(5)	−0.005(7)	3 → 2 → 0	0.00(1)
952.35[a] - sum	−0.309(8)	−0.024(13)	4 → 4 - sum	No
			5 → 4 - sum	−0.39(2)
1052.85[a] - sum	−0.333(12)	−0.065(17)	5 → 4 - sum	−2.9(3)
			4 → 4 - sum	No
1294.55[a] - sum	−0.334(5)	−0.093(14)	3 → 2 - sum	−5.7(6)
			4 → 2 - sum	No
1432.10 - 397.40	0.096(12)	0.015(17)	4 → 2 → 0	

[a]Indicates γ transition for which the mixing has been determined.

III. DISCUSSION

A. Parity doublets versus γ bands

In our previous work on the $N = 86$ isotones we reported on the first observation of γ collectivity in the vicinity of the doubly magic ^{132}Sn core [4]. This picture has been challenged in a recent work [5], which noted that mixing ratios, δ, for decays from the proposed γ band in ^{140}Xe are smaller than expected from the Bohr-Mottelson model. Instead, in Ref. [5] an entirely different picture of a parity-doublet band in an even-

TABLE VI. Experimental angular correlation coefficients, A_k/A_0, and the corresponding mixing ratios, δ, for γ lines in ^{140}Xe, as obtained in the present work. "sum" indicates correlations determined from a spectrum being a sum of γ spectra gated on the 376.7- and 457.8-keV lines.

Cascade E_γ - E_γ	A_2/A_0	A_4/A_0	Spins in cascade	$\delta(\gamma^a)$
381.5 - 738.6[a]	0.117(11)	−0.007(16)	7 → 5 → 4	0.48(4)
				3.4(4)
457.8 - 376.7	0.104(5)	0.000(7)	4 → 2 → 0	
582.4 - sum	0.093(3)	0.004(6)	8 → 6 - sum	
566.6 - sum	0.101(6)	0.023(9)	6 → 4 - sum	
738.6[a] - 457.8	0.214(9)	−0.006(12)	8 → 6 → 4	0.60(5)
			4 → 4 → 2	−0.06(4)
767.9 - sum	−0.072(13)	−0.030(19)	7 → 6 - sum	0.00(3)
820.7[a] - 381.5	0.057(60)	0.038(93)	8 → 7 → 5	0.21(11)
				3.9(15)
			9 → 7 → 5	0.0
891.2[a] - sum	0.092(17)	0.007(23)	6 → 4 - sum	0.0
927.9[a] - 376.7	0.254(20)	0.003(29)	3 → 2 → 0	0.66(20)

[a]Indicates γ transition for which the mixing has been determined.

even nucleus was proposed for ^{140}Xe. This situation needs clarification.

We note that both works [4,5] report the same experimental resuls on ^{140}Xe (this is also stressed in Ref. [5]), while the only essential difference concerns the interpretation. The key structure is a weakly populated sideband comprising the 2775.3-, 3159.7-, and 3730.1-keV levels [4], where Ref. [5] adds two levels at 2282.2 and 2488.9 keV (this extension is not certain because the key 286.4-keV transition linking the 2775.3- and 2488.9-keV levels is very tentative, as seen in Table I of Ref. [5]). More important than the two added levels is the negative parity assignment to levels in this sideband. This parity, crucial for the parity-doublet scenario, was assumed in Ref. [5] without any supporting experimental arguments.

The angular correlations shown in Table VI suggest a positive parity for the 2775.3-keV level because of the nonzero δ of the 820.7-keV transition, though this needs further confirmation, because of a large uncertainty on the δ value. However, there are other arguments against the parity-doublet scenario.

For a parity doublet to occur, a well-developed minimum should be present in the nuclear potential at nonzero β_3. Quantum tunneling between the minima at $+\beta_3$ and $-\beta_3$, produces two solutions corresponding in an even-even nucleus to simplex $s = +1$ and $s = -1$. These solutions are displaced in energy depending on the energy of the tunneling. If the barrier between the two minima is low (shallow octupole minimum) the tunneling is vivid and the $s = -1$ solution is shifted to high energy. Ultimately, only the $s = +1$ solution remains, which is known as the octupole band in nuclei where octupole correlations are present but shapes are reflection symmetric.

Octupole deformation in even-even nuclei of the lanthanide region was reported in barium [7,19] and Sm-Nd isotopes [34,35]. The strength of octupole correlations was estimated to be less than 1 MeV in Ba isotopes [36] and no more than 0.4 MeV in Xe isotopes [37]. Indeed, the electric dipole moments in xenon isotopes are significantly lower than in the barium isotopes, as shown in Fig. 4 of Ref. [18] and as remarked in Ref. [5]. One wonders whether the $s = -1$ solution proposed in ^{140}Xe [5], which is shifted up by about 1.5 MeV, belongs to a ground-state parity doublet created in an octupole well as shallow as 0.4 MeV.

The observation of parity doublets is easier in specific odd-A nuclei, where the proximity of $\Delta j = 3$ Nilsson orbitals may help the picture. This is observed in odd-Z nuclei around $Z = 60$. Parity doublets in ^{151}Pm [38] and ^{153}Eu [39] are quite convincing, with the $s = +i$ and $s = -i$ solutions displaced by about 0.1 MeV only. However, even there the doublet is not yet fully developed and the participating Nilsson orbitals retain their individual properties [39]. This is even worse in ^{145}Ba and ^{147}Ba, where such doublets are not observed [40]. As octupole correlations are still weaker in Xe isotopes, the presence of a parity doublet with the $s = -1$ branch above 2 MeV may be questioned. Till now the $s = -1$ band was proposed in ^{146}Nd [41] and ^{148}Sm [42], but only at spins $I > 10$, where octupole correlations are probably increased by nuclear rotation [43]. At such high excitations some two-quasiparticle excitations of suitable spin and parity may occur and form structures, which can be classified as $s = -1$ bands.

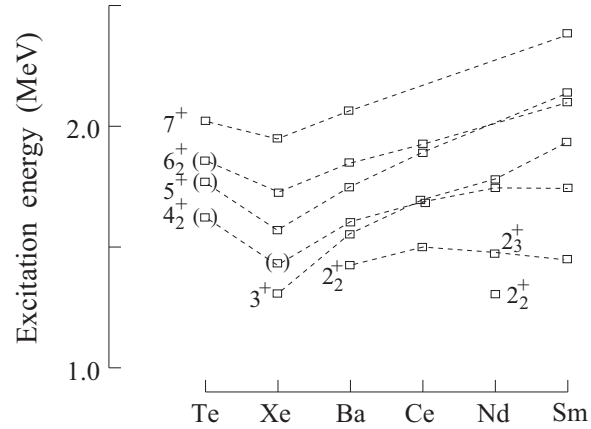

FIG. 8. Energies of positive-parity, yrare levels in $N = 86$ isotones. The data are taken from this work and from Refs. [18,21,42].

Summarizing, we maintain our interpretation of γ bands developing in ^{138}Te and ^{140}Xe, as proposed in Ref. [4]. In the next section we will support this and address the problem of low δ values, with the help of the new data obtained in this work for ^{142}Ba and ^{144}Ce. We note that in case a negative parity is assigned to the 2775.3-keV level in future studies, explanations alternative to a parity doublet are possible; for instance, an octupole phonon coupled to the γ band.

B. Structure of $N = 86$ isotones

The new data obtained in this work allowed the extension of the systematics of positive-parity, yrare levels in the $N = 86$ isotones, shown in Fig. 9(b) of Ref. [4]. The extended systematics, shown in Fig. 8, supports the proposed γ bands at $N = 86$.

In ^{142}Ba a complete, low-spin part of the γ band is now seen. There is also a ground-state octupole band ($s = +1$) but no candidates for the $s = -1$ partner. The sideband starting at 3130.3 keV might be of negative parity (though positive parity is not excluded), but is too high in energy. The new level at 2410.6 keV may have spin 4, as suggested by its decays. The fact that it does not decay to the 2_1^+ level at 359.55 keV could suggest that this level may be due to a double-γ vibration.

The γ band is also observed in ^{144}Ce, starting at the 1489.7-keV level. This level was reported as the head of a γ band in Ref. [44]. The band in ^{144}Ce is shifted to higher energy as compared to ^{140}Xe, making unlikely a parity-doublet scenario involving this band.

The systematics in Fig. 8 indicates a change of the trend in γ bands (the "kink" at Xe) probably caused by a change in the underlying single-particle structure. We also note additional 4^+ and 5^+ levels at comparable energies in the level scheme of ^{144}Ce, which are strongly linked to the γ band and may be due to the Fermi level approaching the $\pi d_{5/2}$ shell. The newly available excitations enrich wave functions, enhancing the collectivity in the γ band and helping a change from what could be called a "proto" γ band in ^{138}Te to a "true" γ band emerging at heavier Z.

Such an evolution is supported by the mixing ratios, δ, shown in Table VII. In ^{138}Te the mixing ratio (known for the

TABLE VII. Mixing ratio, δ, as obtained in this work for transitions depopulating levels in γ bands. Values from Ref. [4][a] and Ref. [5][b] are added to assist the discussion.

	$7_1^+ \to 6_1^+$					
	δ	χ^2/N				
^{138}Te[a]	0.11(3)	0.4				
	6.2(12)	5.6				
	$3_1^+ \to 2_1^+$		$5_1^+ \to 4_1^+$		$5_2^+ \to 4_1^+$	
	δ	χ^2/N	δ	χ^2/N	δ	χ^2/N
^{140}Xe[a]	0.61(15)	0.2	0.50(2)	0.3		
^{140}Xe[b]	0.55(9)		0.53(3)			
	1.3(2)		1.6(1)			
^{140}Xe	0.66(20)	1.0	0.60(5)	0.7		
			1.4(1)	6.9		
^{142}Ba	−3.0(8)	0.2	−0.27(2)	0.2		
	−0.55(10)	2.5	−5.3(5)	22		
^{144}Ce	−5.7(5)	0.9	−0.39(2)	0.3	−0.45(2)	99
	−0.36(2)	35	−3.3(2)	11	−2.9(2)	0.5

$7_1^+ \to 6_1^+$ transition only) has a small, positive value of 0.11. The large value of $\delta = 6.2$ is less likely, as indicated by the χ^2 describing the quality of fitting the formula 1 to the experimental data (it should be explained that, when the uncertainly of the a_4 coefficient is large, which often happens, there are usually two solutions for δ: a small and a large value). The mixing ratio $\delta = +0.52(7)$ for the $3_1^+ \to 2_1^+$ transition in ^{140}Xe is also small and positive, suggesting that there is still a "proto" γ band, as in ^{138}Te. The picture changes in heavier isotones. For the $3_1^+ \to 2_1^+$ transition in ^{142}Ba we obtained $\delta = -3.0(7)$ and in ^{144}Ce $\delta = -5.7(5)$. So, in both nuclei the δ is large (a stronger $E2$ component is present), as expected in a γ band.

Analogous, though somewhat different evolution is seen for the δ values of the $5_1^+ \to 4_1^+$ transition. In ^{142}Ba and ^{144}Ce δ values are still small (though of negative parity), but there is a new effect: in ^{144}Ce the second 4^+ and 5^+ levels have been located and the $5_2^+ \to 4_1^+$ decay has large $\delta = -2.9(2)$. These new levels seen in ^{144}Ce may be due to a "true" γ band mixing with the "proto" γ band.

It is of interest to search for γ bands in heavier-Z, $N = 86$ isotones, particularly in ^{146}Nd. As seen in Fig. 8 the 2_2^+ excitation energy decreases but the 3^+ energy increases when Z is growing. So the level of γ collectivity in not obvious there. In Fig. 8 we assigned the third 2^+ state to the γ band, while proper identification is still in order. As observed at $N > 86$, in some Ba [6,45] and Ce isotopes [44] the second 2^+ level may belong to a β band, which competes here with the γ band.

The concept of "proto" structures has precedents. In a recent work on $A = 86$ isobars [46] a possibile "proto" structure corresponding to mixed-symmetry states in a nucleus with no valence neutrons has been observed. A "bone" structure, similar to a mixed-symmetry states, is formed in ^{86}Kr at the $N = 50$ closed shell by single-particle proton excitations, and is then enriched by proton-neutron coupling at $N > 50$ [47]. This is supported by detailed shell-model calculations [46]. Analogously, the "proto" γ band formed in ^{138}Te evolves into a γ band in ^{144}Ce, when more valence nucleons contribute to the collective motion. Here again the shell model supports the picture, as will be shown in the following section.

IV. SHELL-MODEL CALCULATIONS

In order to get a deeper insight into the new excitation schemes of ^{142}Ba and ^{144}Ce, shell-model calculations are presented in this section with the experimental picture described above in mind.

A. Valence space and effective interaction

The shell-model calculations were performed in the model space $r4h$-$r5i$ spanned by the $2f_{7/2}$, $1h_{9/2}$, $2f_{5/2}$, $3p_{3/2}$, $3p_{1/2}$, $1i_{13/2}$ orbitals for neutrons and the $1g_{7/2}$, $2d_{5/2}$, $2d_{3/2}$, $3s_{1/2}$, $1h_{11/2}$ orbitals for protons, above a closed ^{132}Sn core. The corresponding neutron and proton single-particle energies are taken from ^{133}Sn and ^{133}Sb experimental data [48], respectively. However, the $0i_{13/2}$ neutron and $2s_{1/2}$ proton orbital energies are empirical values from Refs. [49] and [50], respectively.

As a starting point we employed a realistic interaction, derived from chiral effective field theory potentials [51] denoted N3LO. Its short-range repulsion was renormalized through the low-momentum potential $V_{\text{low-}k}$ with a cutoff $\Lambda = 2.2$ fm^{-1}. This renormalized interaction was adapted to the model space by many body perturbation theory techniques, including all the $\hat{Q}$-box folded diagrams up to the second order [52].

In the second step we reduced slightly (by about 120 keV) the $1f_{7/2}$ neutron-neutron pairing matrix element of the realistic interaction, to reproduce isomeric transitions in ^{134,136,138}Sn isotopes following [1,12,13]. Hereafter, we name the resulting effective interaction N3LOP, and apply it to survey the properties of ^{142}Ba and ^{144}Ce nuclei.

The diagonalization using the ANTOINE shell-model code [53,54] was confronted with the large dimension of the Hamiltonian matrices (3×10^9 in ^{142}Ba and 3×10^{10} in ^{144}Ce). Truncation was necessary in the case of ^{144}Ce, keeping up to 6p-6h excitations, while the full configurations space is included in ^{142}Ba.

B. Results and discussions

The energy levels in both nuclei calculated using the N3LOP interaction are compared to the experimental data in Figs. 9 and 10. The reproduction is very good for all states of ^{142}Ba and ^{144}Ce shown. The compression of some excited states energies in ^{144}Ce is understood as an effect of the truncation. We checked, however, that the adopted truncations ensure the good convergence of energy levels and preserve the collective properties of both nuclei.

In ^{142}Ba the results support the tentative 9^+ and 11^+ spin and parity assignments to levels at 2680.0 and 3342.8 keV, which are calculated at 2727.7 and 3452.4 keV, respectively. Two experimental levels at 3507.3 and 3965.1 keV coincide with the 12^+ and 13^+ states calculated at 3575.1 and 4339.9 keV, respectively. Similarly, in ^{144}Ce the tentative 6^+ assignment to the new level at 1923.6 keV is supported by the corresponding theoretical level at 1960.3 keV. We also confirm experimental 5^+ states at 1891.0 and 1991.5 keV, which are calculated at

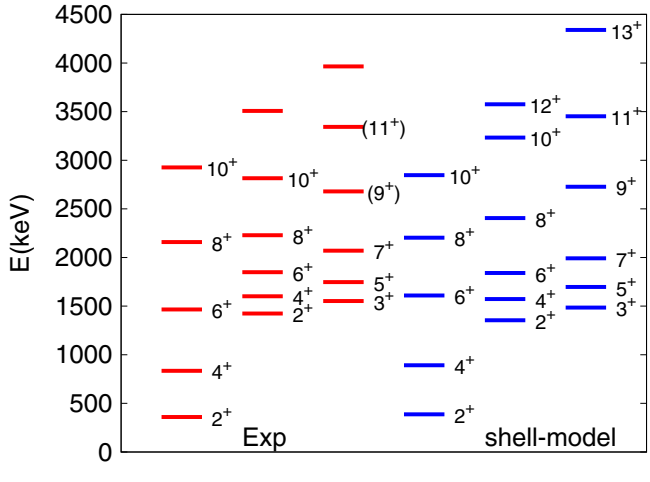

FIG. 9. Excited levels in ^{142}Ba calculated using the N3LOP effective interaction (blue lines), compared to the experimental scheme (red lines).

1797.5 and 1899.2 keV, respectively. The energies of the not yet observed 7_1^+ and 8_2^+ states are predicted at 2067.3 and 2713.2 keV.

The electromagnetic properties of both nuclei are displayed in Table VIII. Magnetic moments of 2_1^+ levels are calculated using the spin and orbital g factors, $(g_\pi^s, g_\pi^l) = (3.250, 1.069)$ for protons and $(g_\nu^s, g_\nu^l) = (-1.506, 0.019)$ for neutrons. These values are adjusted to reproduce the available data for the magnetic moments of $N = 82,84,86$ isotones [55]. This renormalization accounts for the lack of the spin-orbit partners in our model space. In this case, the calculated value in ^{142}Ba is in a better agreement with the data, as compared to the previously calculated value $\mu(2^+) = 0.61\mu_N$ from Ref. [15].

An important result of our shell-model calculations is the reproduction of collectivity in the $N = 86$ isotones, suggested by the experiment, as discussed in Sec. III B. The analysis of transition rates reveals strong $B(E2; 2^+ \rightarrow 0^+)$ values (see

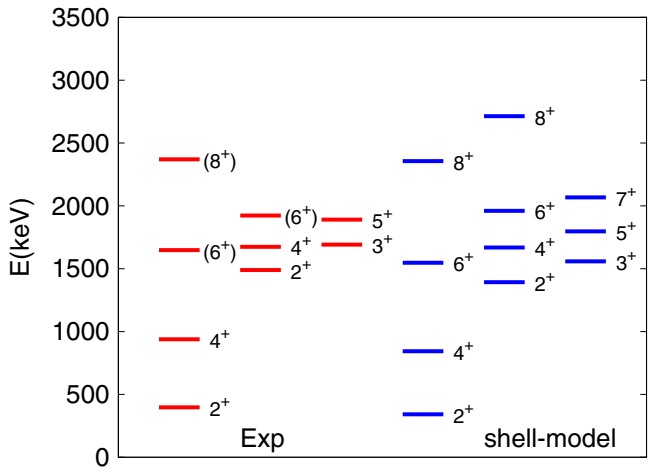

FIG. 10. Excited levels in ^{144}Ce calculated using the N3LOP effective interaction (blue lines), compared to the experimental scheme (red lines).

TABLE VIII. Electromagnetic properties of ^{142}Ba and ^{144}Ce: Quadrupole moments, $E2$ transition rates (calculated using $0.6e$ and $1.6e$ effective charges for neutrons and protons, respectively), and the magnetic moment. See also the text for the g-factor values.

	^{142}Ba	^{144}Ce
Shell model		
$Q_s(2_1^+)$ e fm^2	−74.6	−80.2
$Q_s(2_2^+)$ e fm^2	67.9	75.1
$Q_s(3^+)$ e fm^2	−1.12	−7.23
$BE2(2_1^+ \rightarrow 0^+)$ e^2 fm^4	1458	1620
$BE2(3^+ \rightarrow 2_2^+)$ e^2 fm^4	1688	2419
$\mu(2_1^+)\mu_N$	0.799	0.788
Experiment		
$BE2(2_1^+ \rightarrow 0^+)$ e^2 fm^4	1352(70)	1920(480)
$\mu(2_1^+)\mu_N$	0.852(10)	
Q_i from Q_s		
$Q_i(2_1^+)$ e fm^2	261	280
$Q_i(4_1^+)$ e fm^2	276	288
$Q_i(6_1^+)$ e fm^2	285	287
Q_i from $B(E2)$		
$Q_i(2_1^+)$ e fm^2	271	285
$Q_i(4_1^+)$ e fm^2	274	288
$Q_i(6_1^+)$ e fm^2	271	286

Table VIII). The $E(4^+)/E(2^+) \sim 2.4$ energy ratio is typical for transitional nuclei. There are also low-energy 2_2^+ states. These aspects constitute clues of the presence of significant quadrupole correlations.

Using the Bohr-Mottelson collective model [56], the transformation of quadrupole properties from the laboratory to the intrinsic frame is expressed as

$$Q_i = \frac{(J+1)(2J+3)}{3K^2 - J(J+1)} Q_s(J), \quad K \neq 1, \tag{3}$$

$$BE2(J \rightarrow J-2) = \frac{5e^2}{16\pi} |\langle JK20|J-2,K\rangle|^2 Q_i^2, \quad K \neq \frac{1}{2}, 1. \tag{4}$$

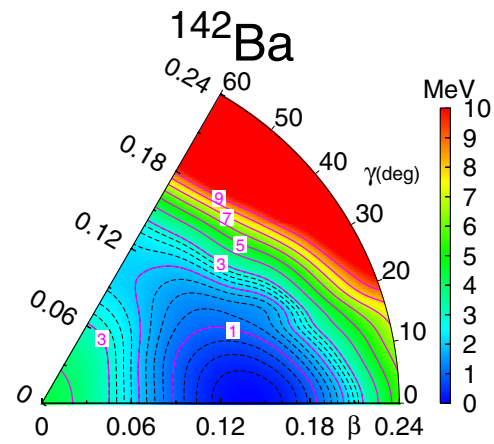

FIG. 11. Potential energy surface of ^{142}Ba in the β-γ plane calculated using CHFSM.

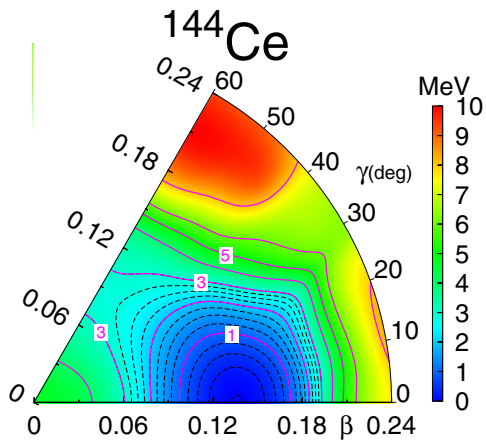

FIG. 12. Potential energy surface of ^{144}Ce in the β-γ plane calculated using CHFSM.

The investigation of the spectroscopic quadrupole properties of both systems (listed in Table VIII) suggests the presence of $K = 2$ γ bands:

(1) $Q_s(2^+_\gamma, K = 2)$ is nearly equal to $Q_s(2^+, K = 0)$ but has an opposite sign.
(2) $Q_s(3^+, K = 2)$ is close to zero and the low-lying 3^+ state is connected by a strong transition to the 2^+_γ state.

In Table VIII we extracted the intrinsic quadrupole moments Q_i from the $B(E2)$ values and from the spectroscopic quadrupole moments Q_s of the 2^+, 4^+, and 6^+ yrast states. We conclude that the results are compatible with deformed intrinsic states with nearly constant quadrupole moments.

In order to provide further insight into the deformation and the intrinsic shapes of these nuclei we calculated the usual β and γ deformation parameters using Kumar's geometrical model. They are defined as a function of diagonal and nondiagonal $E2$ sum rules [57]. The set of β and γ values ascribed to ^{142}Ba $(0.18, 15^\circ)$ and ^{144}Ce $(0.18, 16^\circ)$ indicate nonaxiality in both nuclei.

To confirm our deformation analysis, the potential energy surfaces (PES) were obtained from the constrained Hartree-Fock calculations within the shell-model basis [58], using the same shell-model Hamiltonian and the same valence space. The PES maps displayed in Figs. 11 and 12, in the β-γ plane ($0 \leqslant \gamma \leqslant 60^\circ$), reveal large minima extending towards nonzero γ, supporting the picture of γ softness bands in both nuclei.

From our study of $N = 82$, 84, and 86 isotones with $52 \leqslant Z \leqslant 60$ [15] we infer that the deformation regime starts at $N = 86$ isotones and increases clearly from ^{140}Xe to ^{146}Nd. This enhancement of the collectivity is interpreted as the result of the interplay of pseudo-SU(3) symmetry [59] of the $g_{7/2}, d_{5/2}, d_{3/2}, s_{1/2}$ proton orbitals sequence and quasi-SU(3) symmetry [60,61] of the $f_{7/2}, p_{3/2}$ neutron orbitals sequence.

V. CONCLUSIONS

Summarizing, the excitation schemes of ^{142}Ba and ^{144}Ce were extended and firm spin-parity assignments were obtained for several excited levels in both nuclei, based on angular correlations following spontaneous fission of ^{252}Cf. The new results support the presence of γ bands in both nuclei, which develop here better than in ^{138}Te and ^{140}Xe [4]. This evolution is supported, among other experimental observables, by the increase of the mixing ratios, δ, when going from ^{138}Te to ^{144}Ce.

The shell-model calculations, performed in this work using the N3LOP effective interaction, support the presence of γ bands in the $N = 86$ isotones. The calculated electromagnetic properties of ^{142}Ba and ^{144}Ce are fully consistent with the experimental signatures of γ collectivity in both nuclei.

Thus, contrary to a recent claim of parity doublets in ^{140}Xe [5], the results of the present work and of our previous studies [4,15], fully support the interpretation of γ collectivity at $N = 86$, where both schemes of experimental and theoretical levels, as well the calculated quadrupole properties, display patterns characteristic of soft, triaxial shapes in both nuclei. According to the shell-model calculations [15], the evolution of the collectivity in this mass region is sensitive to the SU(3) symmetries structure of neutron and proton orbitals.

It is of interest to further verify the proposed effects, by searching for γ bands at higher Z number in $N = 86$ isotones as well as tracing their development with the increasing neutron number, along isotopic lines in Xe, Ba, and Ce nuclei.

Finally, we note that the presence of ground-state octupole bands and γ collectivity at $N = 86$ opens up an interesting field of studying the interplay between these two types of excitations.

[1] G. S. Simpson, G. Gey, A. Jungclaus, J. Taprogge, S. Nishimura, K. Sieja, P. Doornenbal, G. Lorusso, P.-A. Söderström, T. Sumikama *et al.*, Phys. Rev. Lett. **113**, 132502 (2014).
[2] P. Lee, C.-B. Moon, C. S. Lee, A. Odahara, R. Lozeva, A. Yagi, S. Nishimura, P. Doornenbal, G. Lorusso, P.-A. Söderström *et al.*, Phys. Rev. C **92**, 044320 (2015).
[3] R. Lozeva, H. Naïdja, F. Nowacki, J. Dudek, A. Odahara, C.-B. Moon, S. Nishimura, P. Doornenbal, J.-M. Daugas, P.-A. Söderström *et al.*, Phys. Rev. C **93**, 014316 (2016).
[4] W. Urban, K. Sieja, T. Rząca-Urban, M. Czerwiński, H. Naïdja, F. Nowacki, A. G. Smith, and I. Ahmad, Phys. Rev. C **93**, 034326 (2016).
[5] Y. Huang, S. J. Zhu, J. H. Hamilton, E. H. Wang, A. V. Ramayya, Z. G. Xiao, H. J. Li, Y. X. Luo, J. O. Rasmussen, G. M. Ter-Akopian, and Y. T Oganessian, Phys. Rev. C **93**, 064321 (2016).
[6] A. J. Mitchell, C. J. Lister, E. A. McCutchan, M. Albers, A. D. Ayangeakaa, P. F. Bertone, M. P. Carpenter, C. J. Chiara, P. Chowdhury, J. A. Clark *et al.*, Phys. Rev. C **93**, 014306 (2016).
[7] B. Bucher, S. Zhu, S. Y. Wang, R. A. Bark, S. Q. Zhang, J. Meng, B. Qi, 1 P. Jones, S. M. Wyngaardt, J. Zhao *et al.*, Phys. Rev. Lett. **116**, 112503 (2016).
[8] S. Ilieva, T. Kröll, J.-M. Régis, N. Saed-Samii, A. Blanc, A. M. Bruce, L. M. Fraile, G. de France, A.-L. Hartig, C. Henrich,

A. Ignatov, M. Jentschel, J. Jolie, W. Korten, U. Köster, S. Lalkovski, R. Lozeva, H. Mach, N. Märginean, P. Mutti, V. Paziy, P. H. Regan, G. S. Simpson, T. Soldner, M. Thürauf, C. A. Ur, W. Urban, and N. Warr, Phys. Rev. C **94**, 034302 (2016).
[9] D. Bianco, N. Lo Iudice, F. Andreozzi, A. Porrino, and F. Knapp, Phys. Rev. C **88**, 024303 (2013).
[10] S. Sarkar and M. Saha Sarkar, Phys. Rev. C **81**, 064328 (2010).
[11] A. Covello, L. Corragio *et al.*, Prog. Part. Nucl. Phys. **59**, 401 (2007).
[12] H. Naïdja, F. Nowacki, and K. Sieja, J. Phys.: Conf. Ser. **580**, 012030 (2015).
[13] H. Naïdja, F. Nowacki, and K. Sieja, Acta Phys. Pol. B **46**, 669 (2015).
[14] K. Sieja, Acta Phys. Pol. B **47**, 883 (2016).
[15] H. Naïdja and F. Nowacki, Acta Phys. Pol. B **48**, 587 (2017).
[16] R. N. Bernard, L. M. Robledo, and T. R. Rodríguez, Phys. Rev. C **93**, 061302(R) (2016).
[17] A. Lindroth, B. Fogelberg, H. Mach, M. Sanchez-Vega, and J. Bielčik, Phys. Rev. Lett. **82**, 4783 (1999).
[18] W. Urban, T. Rząca-Urban, N. Shulz, J. L. Durell, W. R. Phillips, A. G. Smith, B. J. Varley, and I. Ahmad, Eur. Phys. J. A **16**, 303 (2003).
[19] W. R. Phillips, I. Ahmad, H. Emling, R. Holzmann, R. V. F. Janssens, T.-L. Khoo, and M. W. Drigert, Phys. Rev. Lett. **57**, 3257 (1986).
[20] M. A. Jones, W. Urban, J. L. Durell, M. J. Leddy, W. R. Phillips, A. G. Smith, B. J. Varley, I. Ahmad, L. R. Morss, M. Bentaleb, E. Lubkiewicz, and N. Schulz, Nucl. Phys. A **605**, 133 (1996).
[21] W. Urban, M. A. Jones, J. L. Durell, M. J. Leddy, W. R. Phillips, A. G. Smith, B. J. Varley, I. Ahmad, L. R. Morss, M. Bentaleb, E. Lubkiewicz, and N. Schulz, Nucl. Phys. A **613**, 107 (1997).
[22] S. J. Zhu, Q. H. Lu, J. H. Hamilton, A. V. Ramayya, L. K. Peker, M. G. Wang, W. C. Ma, B. R. S. Babu, T. N. Ginter, J. Kormicki, D. Shi, J. K. Deng, W. Nazarewicz, J. O. Rasmussen, M. A. Stoyer *et al.*, Phys. Lett. B **357**, 273 (1995).
[23] D. Patel, A. G. Smith, G. S. Simpson, R. M. Wall, J. F. Smith, O. J. Onakanmi, I. Ahmad, J. P. Greene, M. P. Carpenter, T. Lauritsen, C. J. Lister, R. F. Janssens, F. G. Kondev, D. Seweryniak, B. J. P. Gall, O. Dorveaux, and B. Roux, J. Phys. G: Nucl. Part. Phys. **28**, 649 (2002).
[24] R. Orlandi, A. G. Smith, D. Patel, G. S. Simpson, R. M. Wall, J. F. Smith, O. J. Onakanmi, I. Ahmad, J. P. Greene, M. P. Carpenter, T. Lauritsen, C. J. Lister, R. V. F. Janssens, F. G. Kondev, D. Seweryniak, B. J. P. Gall, O. Dorveaux, and A. E. Stuchbery, Phys. Rev. C **73**, 054310 (2006).
[25] W. Urban, M. Jentschel, B. Märkisch, Th. Materna, Ch. Bernards, C. Drescher, Ch. Fransen, J. Jolie, U. Köster, P. Mutti, T. Rząca-Urban, and G. S. Simpson, J. Instrum. **8**, P03014 (2013).
[26] K. S. Krane, R. M. Steffen, and R. M. Wheeler, Nucl. Data Tables **11**, 351 (1973).
[27] W. D. Hamilton, in *The Electromagnetic Interaction in Nuclear Spectroscopy*, edited by W. D. Hamilton (North-Holland, Amsterdam, 1975), Chap. 14.
[28] https://www.phy.anl.gov/gammasphere/.
[29] C. Goodin, A. V. Ramayya, J. H. Hamilton, N. J. Stone, A. V. Daniel, K. Li, S. H. Liu, J. K. Hwang, Y. X. Luo, J. O. Rasmussen, and S. J. Zhu, Phys. Rev. C **80**, 014318 (2009).
[30] M. Czerwiński, Ph.D. thesis, University of Warsaw, 2017 (unpublished).
[31] T. D. Johnson, D. Symochko, M. Fadil, and J. K. Tuli, Nucl. Data Sheets **112**, 1949 (2011).
[32] I. Ahmad and W. R. Phillips, Rep. Prog. Phys. **58**, 1415 (1995).
[33] A. A. Sonzogni, Nucl. Data Sheets **93**, 599 (2000).
[34] W. Urban, R. M. Lieder, W. Gast, G. Hebbinghaus, A. Krämer-Flecken, K. P. Blume, and H. Hübel, Phys. Lett. B **185**, 331 (1987).
[35] W. Urban, R. M. Lieder, W. Gast, G. Hebbinghaus, A. Krämer-Flecken, T. Morek, T. Rzaca-Urban, W. Nazarewicz, and S. L. Tabor, Phys. Lett. B **200**, 424 (1988).
[36] G. A. Leander, W. Nazarewicz, P. Olanders, I. Ragnarsson, and J. Dudek, Phys. Lett. B **152**, 284 (1985).
[37] M. Bentaleb, N. Schulz, E. Lubkiewicz, J. L. Durell, C. J. Pearson, W. R. Phillips, J. Shannon, B. J. Varley, I. Ahmad, C. J. Lister, L. R. Morss, K. L. Nash, and C. W. Williams, Z. Phys. A **354**, 143 (1996).
[38] W. Urban, J. C. Bacelar, W. Gast, G. Hebbinghaus, A. Krämer-Flecken, R. M. Lieder, T. Morek, and T. Rząca-Urban, Phys. Lett. B **247**, 238 (1990).
[39] C. J. Pearson, W. R. Phillips, J. L. Durell, B. J. Varley, W. J. Vermeer, W. Urban, and M. K. Khan, Phys. Rev. C **49**, R1239 (1994).
[40] T. Rząca-Urban, W. Urban, A. G. Smith, I. Ahmad, and A. Syntfeld-Każuch, Phys. Rev. C **87**, 031305(R) (2013).
[41] V. Iacob, W. Urban, J. C. Bacelar, J. R. Jongman, J. Nyberg, G. Sletten, and L. Trache, Nucl. Phys. A **596**, 155 (1996).
[42] W. Urban, R. M. Lieder, J. C. Bacelar, P. P. Singh, D. Alber, D. Balabanski, W. Gast, H. Grawe, J. R. Jongman, G. Hebbinghaus, T. Morek, R. F. Noorman, T. Rzaca-Urban, H. Schnare, M. Thoms, O. Zell, and W. Nazarewicz, Phys. Lett. B **258**, 293 (1991).
[43] W. Nazarewicz, G. A. Leander, and J. Dudek, Nucl. Phys. A **467**, 437 (1987).
[44] S. Yamada, A. Taniguchi, K. Okano, and K. Aoki, Eur. Phys. J. A **7**, 327 (2000).
[45] J. B. Gupta and M. Saxena, Phys. Rev. C **91**, 054312 (2015).
[46] W. Urban, K. Sieja, T. Materna, M. Czerwiński, T. Rząca-Urban, A. Blanc, M. Jentschel, P. Mutti, U. Köster, T. Soldner, G. de France, G. S. Simpson, C. A. Ur, C. Bernards, C. Fransen, J. Jolie, J.-M. Regis, T. Thomas, and N. Warr, Phys. Rev. C **94**, 044328 (2016).
[47] T. Thomas, V. Werner, J. Jolie, K. Nomura. T. Ahn, N. Cooper, H. Duckwitz, A. Fitzler, C. Fransen, A. Gade, M. Hinton, G. Ilie, J. Jenssen, A Linnemann, P. Petkov, N. Pietralla, and D. Radeck, Nucl. Phys. A **947**, 203 (2016).
[48] NNDC, National Nuclear Data Center, Brookhaven National Laboratory, http://www.nndc.bnl.gov.
[49] W. Urban, W. Kurcewicz, A. Nowak, T. Rzaca-Urban *et al.*, Eur. Phys. J. **5**, 239 (1999).
[50] F. Andreozzi, L. Coraggio, A. Covello, A. Gargano, T. T. S. Kuo, and A. Porrino, Phys. Rev. C **56**, R16 (1997).
[51] D. R. Entem and R. Machleidt, Phys. Rev. C **68**, 041001 (2003).
[52] M. Hjorth-Jensen, T. T. S. Kuo, and E. Osnes, Rev. Rep. **261**, 125 (1995).
[53] E. Caurier, G. Martinez-Pinedo, F. Nowacki, A. Poves, and A. P. Zuker, Rev. Mod. Phys. **77**, 427 (2005).
[54] E. Caurier and F. Nowacki, Acta Phys. Pol. B **30**, 705 (1999).

[55] N. J. Stone, At. Data Nucl. Data Tables **90**, 75 (2005).
[56] A. Bohr and B. R. Mottelson, K. Dan. Vidensk. Selsk. Mat. Fys. Medd. **27**, 16 (1953).
[57] K. Kumar, Phys. Rev. Lett. **28**, 249 (1972).
[58] B. Bounthong, Ph.D. thesis, Université de Strasbourg, 2016 (unpublished).
[59] E. Caurier, F. Nowacki, A. Poves, and K. Sieja, Phys. Rev. C **82**, 064304 (2010).
[60] A. P. Zuker, J. Retamosa, A. Poves, and E. Caurier, Phys. Rev. C **52**, R1741 (1995).
[61] A. P. Zuker, A. Poves, F. Nowacki, and S. M. Lenzi, Phys. Rev. C **92**, 024320 (2015).